Ureteric stents: investigating flow and encrustation

S L Waters[1]*, K Heaton[2], J H Siggers[3], R Bayston[2], M Bishop[4], L J Cummings[1], D M Grant[5], J M Oliver[1], and **J A D Wattis[1]**
[1]Division of Applied Mathematics, University of Nottingham, Nottingham, UK
[2]School of Medical and Surgical Sciences, University of Nottingham, Nottingham, UK
[3]Department of Bioengineering, Imperial College London, London, UK
[4]City Hospital Nottingham, Nottingham, UK
[5]School of Mechanical, Materials and Manufacturing Engineering, University of Nottingham, Nottingham, UK

The manuscript was received on 6 April 2007 and was accepted after revision for publication on 9 January 2008.

DOI: 10.1243/09544119JEIM317

Abstract: Blockages of the ureter, e.g. due to calculi (kidney stones), can result in an increase in renal pelvic pressure. This may be relieved by inserting a stent (essentially a permeable hollow tube). However, a number of complications are associated with stent use. Stents can result in reflux (backflow of urine along the ureter), which will promote recurrent urinary infection and possible renal parenchymal damage. Furthermore, long-term stent use is associated with infection and precipitation of salts from the urine, which can lead to a build-up of crystalline deposits on the stent surface, making stent removal difficult and painful. This paper examines factors governing urine flow in a stented ureter, the implications for reflux, and the processes by which the stent surface encrusts, in particular focusing on the influence of bacterial infection. An interdisciplinary approach is adopted, involving a combination of theoretical investigations and novel experiments.

Keywords: urinary tract, ureteric stents, reflux, encrustation

1 INTRODUCTION

The urinary tract is a conduit and reservoir for urine excreted by the kidney. After production in the renal parenchyma, urine collects in the funnel-shaped renal pelvis of the kidney and passes down the ureter to the bladder, where it is stored at low pressure until micturition occurs. During voiding the bladder pressure rises, driving urine flow through the urethra and out of the body. The junctions between the renal pelvis and the ureter, and the ureter and the bladder, are referred to as the ureteropelvic junction (UPJ) and the vesicoureteric junction (VUJ) respectively. Under normal conditions, the VUJ closes during voiding to prevent reflux (back flow) of urine up the ureter.

Urine is mostly water and contains electrolytes, urea and other more complex waste products of protein metabolism, and a little albumin. It is usually supersaturated, but in normal individuals inhibitors prevent crystallization and aggregation [**1**]. The urine in the bladder is more concentrated and of higher pH than urine in the renal pelvis [**2**, **3**] and, while levels of bacteria in urine are normally very low (less than 10^3 per mm^3), the counts are usually higher in the bladder than in the renal pelvis, presumably because most bacterial colonization is derived from organisms populating the bowel and perineum.

In a healthy system, rhythmic coordinated contractions of the ureter (peristalsis) push urine down the ureter to the bladder at flowrates in the range 0.5–10 ml/min for each kidney/ureter [**4**]. However, the ureter may become blocked, either internally (e.g. by a calculus) or by external compression (e.g. from a tumour) and occasionally an obstruction can develop rapidly and become life threatening, either owing to increased intrarenal pressure (which may stop urine production and over time cause kidney failure) or by causing an infection. Ideally, the obstruction should be removed, but if this is not

**Corresponding author: Mathematics Institute, University of Oxford, 24–29 St Giles', Oxford, OX1 3LB, UK. email: waters@maths.ox.ac.uk*

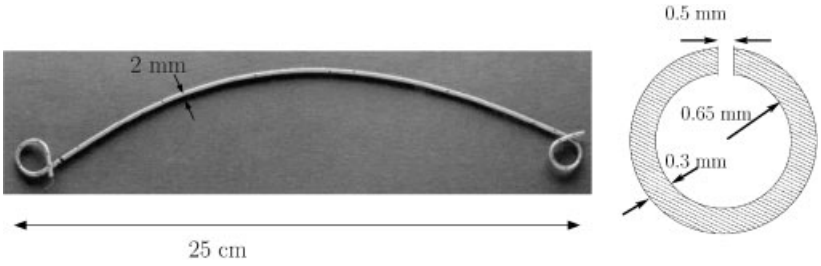

Fig. 1 (a) Double-pigtail stent (taken from www.bui.ac.uk). (b) Cross-section of a double-pigtail stent, illustrating the presence of holes in the stent wall. Typical stent dimensions are shown

possible, the pressure must be relieved, by direct drainage of the kidney (a nephrostomy) or via the insertion of a stent.

Clinically, a number of different stent designs are available [**4**]: double-pigtail stents made of polymers such as polyethylene and ethyl vinyl acetate often with a hydrogel coating, which extend the entire length of the ureter (see Fig. 1), and a range of shorter metal stents, which sit at the blockage site. The double-pigtail stent is a flexible tube of length 25 cm, usually punctuated with holes of diameter approximately 0.5 mm along its length. The internal and external tube diameters can vary, but a typical internal diameter is 1.3 mm and the tube wall thickness is 0.3 mm (measured from stents supplied by Boston Scientific, Natick, Massachusetts)*. The stent is relatively pliable longitudinally, but difficult to compress radially. Curls at each end anchor the lower end in the bladder and the upper end in the renal pelvis [**5**].

A number of complications are associated with stent use. First, irritation of the bladder due to the presence of the stent can result in short-duration detrusor contractions, leading to a transient rise in bladder pressure (a spasm) [**6**]. Second, the VUJ is held open by the stent, allowing urine to reflux whenever the bladder pressure rises, e.g. during voiding or a spasm. Finally, long-term stent use is associated with infection, and precipitation of some salts in the urine, which can lead to a build-up of crystalline deposits on the stent surface [**6**]. Encrustation can lead to further blockages of the system, making stent removal difficult and painful, if the encrustation is severe.

This paper briefly summarizes aspects of interdisciplinary work to understand and predict the causes of ureteric stent failure. In section 2 an investigation of urine flow in a stented ureter is presented, which is used to quantify reflux. In section 3 the relationship between bacterial flora and ureteric stent encrustation is examined. Finally, in section 4 details of ongoing work in this field are briefly discussed.

*Note that commonly stent sizes are quoted in French (Fr), where a stent of size x Fr has an external diameter of x/π mm.

2 URINE FLOW IN A STENTED URETER

Studies have shown that peristalsis can be suppressed (often strongly) in the stented ureter, so that passive draining is the principal mode of urine transport [**7**], and the possibility of reflux becomes an important issue. To determine how the degree of reflux during voiding is affected by the ability of the stent to transmit fluid both axially and transversely (across its walls), Cummings *et al.* [**8**] studied an axisymmetric model of a stented ureter. The ureter wall was assumed to be linearly elastic and asymptotic methods were employed to determine the flow when the reduced bladder pressure is slightly higher than the reduced pressure in the renal pelvis (reduced pressure is defined as the absolute pressure minus the hydrostatic pressure contribution). This initial model predicted that a highly permeable stent gives rise to less reflux than an impermeable one. However, the model neglected the non-linear elastic properties of the ureter wall and did not accurately account for the physiologically realistic pressures and parameters, or axial variations in the material properties of the ureter and the stent (e.g. due to encrustation or blockages).

2.1 Theoretical model

In this section, a model is developed that accounts for the key components of the stented urinary tract: stent, ureter, renal pelvis, and bladder. The model is used to quantify reflux. A schematic diagram is shown in Fig. 2. Details of the full model derivation are given in reference [**9**]; a simplified version is

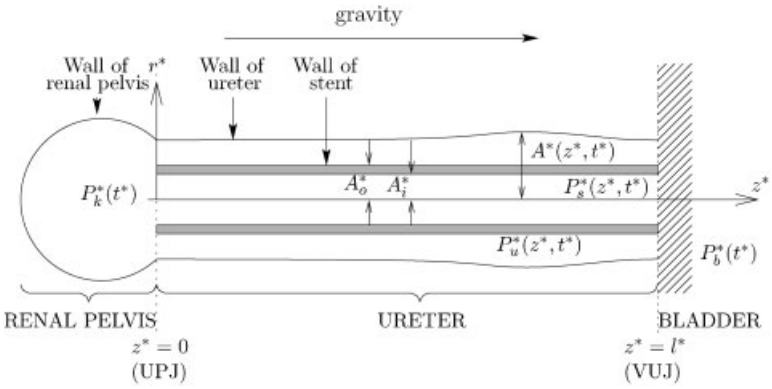

Fig. 2 Schematic diagram of the model showing the ureter, stent, and renal pelvis

presented here that does not account for axial stretch of the ureter wall, urine production by the kidney, or axial variations in, for example, the ureter wall material properties or stent geometry.

A cylindrical polar coordinate system (r^*, z^*) is adopted. The urine is assumed to be a homogeneous, incompressible, Newtonian viscous fluid, with viscosity μ^* and density ρ^* of water. The presence of the stent causes the ureter wall to lose muscle tone and expand, and consequently the ureter and stent are assumed to be axisymmetric, with a common axis. The ureter (and stent) are of length l^*, and $A^*(z^*, t^*)$ is the ureter cross-sectional area, where t^* is time. The UPJ is at $z^* = 0$ and the VUJ is at $z^* = l^*$. Ureteric pressures inside and outside the stent are denoted P_{s}^* and P_{u}^* respectively. The flux within the ureter (which has components due to flow both inside and outside the stent) is denoted by q^*. The fact that both the aspect ratio (the ratio of typical ureter radius to length) and the reduced Reynolds number of the flow are small is expected; the fluid flow may then be approximated using lubrication theory in which the fluid inertia is neglected and the fluid pressure is independent of the radial coordinate [**10**]. The stent is modelled as a rigid, permeable tube with circular cross-section. The stent has uniform inner and outer cross-sectional areas A_{i}^* and A_{o}^* respectively, and the flux of urine across the stent wall (per unit length) is proportional to the pressure difference across the wall, with constant of proportionality d^* (permeability).

Supposing that peristalsis is suppressed in a stented ureter [**7**], active wall contractions are neglected and the ureter wall is modelled as an elastic membrane with natural (unstretched) cross-sectional area A_{a}^*. The ureter wall is assumed to move only in the radial direction and the membrane tension is assumed to be a non-linear function of the radial stretch, denoted $f^*\left(\sqrt{A^*/A_{\mathrm{a}}{}^*}\right)$, where (see reference [**11**] for details)

$$f^*\left(\sqrt{A^*/A_{\mathrm{a}}{}^*}\right) = k^*\left(\mathrm{e}^{\gamma\left(\sqrt{A^*/A_{\mathrm{a}}{}^*}-1\right)}-1\right) \tag{1}$$

Here k^* characterizes the stiffness of the ureter wall and γ captures how rapidly the membrane tension varies with ureter radius. The timescale over which the ureter wall achieves equilibrium is assumed to be much shorter than the flow timescale, and hence wall inertia is neglected. The stented ureter system is taken to be vertically upright and the pressure external to the ureter is assumed to be hydrostatic, P_{hyd}^*. The renal pelvis is modelled as an elastic bag of constant bulk stiffness k_k^*, with fluid pressure $P_k^*(t^*)$, and it is assumed that the time-rate of change of pressure within it depends linearly on the flux of fluid through the UPJ. At either end of the ureter the pressures inside and outside the stent are taken to be equal: at $z^* = 0$ they are $P_k^*(t^*)$ and at the bladder ($z^* = l^*$) they equal $P_{\mathrm{b}}^*(t^*)$, the bladder pressure, which is prescribed and drives the fluid flow.

The reduced pressure p^* is defined as $p^* = P^* - P_{\mathrm{hyd}}^*$. Initially, the reduced pressures in the renal pelvis and the bladder are equated to zero, the fluid is stationary, and the ureter cross-sectional area is equal to A_{a}^*. The rise and subsequent fall back to zero of the bladder pressure due to voiding or a spasm is modelled as $P_{\mathrm{b,max}}^* \sin^2(\pi t^*/\tau^*)$, so that the pulse has amplitude $P_{\mathrm{b,max}}^*$ and duration τ^*. A range of values for $P_{\mathrm{b,max}}^*$ and τ^* are considered.

2.2 Dimensionless governing equations and boundary conditions

For a full derivation of the governing equations see reference [**9**]. Pressures are non-dimensionalized

with respect to $P^*_{\mathrm{b,max}}$. The remaining variables are non-dimensionalized as follows

$$z^* = l^* z, \quad (A^*, A_\mathrm{i}^*, A_\mathrm{o}^*) = A_\mathrm{a}^*(A, A_\mathrm{i}, A_\mathrm{o}),$$
$$q^* = (l^* A_\mathrm{a}^*/\tau^*)q, \quad t^* = \tau^* t \tag{2}$$

After non-dimensionalizing, the dimensionless parameters, in addition to γ, are

$$k = \frac{\sqrt{\pi}k^*}{\sqrt{A_\mathrm{a}^* P^*_{\mathrm{b,max}}}}, \quad k_k = \frac{A_\mathrm{a}^* l^* k_k^*}{P^*_{\mathrm{b,max}}},$$

$$D = \frac{\sqrt{A_\mathrm{a}^*}k^*\tau^*}{8\sqrt{\pi}\mu^* l^{*2}}, \quad d = \frac{8\pi\mu^* d^* l^{*2}}{A_l^{*2}} \tag{3}$$

In definitions (3), k and k_k are the dimensionless stiffness of the ureter and the renal pelvis respectively, D represents the ratio of the pulse duration to the timescale over which the ureter wall relaxes, and d is the dimensionless stent permeability.

The system reduces to two dimensionless equations for the dependent variables A and p_s

$$\frac{\partial A}{\partial t} + \frac{\partial q}{\partial z} = 0 \tag{4a}$$

$$\frac{\partial^2 p_\mathrm{s}}{\partial z^2} - d(p_\mathrm{s} - p_\mathrm{u}) = 0 \tag{4b}$$

where

$$q = -\frac{D}{k}\left\{(A - A_\mathrm{o})\left[A + A_\mathrm{o} - \frac{2(A - A_\mathrm{o})}{\ln(A/A_\mathrm{o})}\right]\frac{\partial p_\mathrm{u}}{\partial z} + A_i^2 \frac{\partial p_\mathrm{s}}{\partial z}\right\} \tag{5a}$$

$$p_\mathrm{u} = \frac{k}{\sqrt{A}}\left(\mathrm{e}^{\gamma(\sqrt{A}-1)} - 1\right) \tag{5b}$$

Equation (4a) represents conservation of mass while equation (4b) is derived from the conservation of momentum equations, for the fluid within and outside the stent, exploiting the fact that the aspect ratio and reduced Reynolds number are too small to obtain a simplified approximate system (lubrication theory) [**9**].

Equations (4) and (5) are solved subject to the following axial boundary conditions

$$p_\mathrm{s} = p_\mathrm{u} \quad \text{at } z = 0, \tag{6a}$$

$$\frac{\partial p_\mathrm{u}}{\partial t} = -k_k q \quad \text{at } z = 0, \tag{6b}$$

$$p_\mathrm{s} = p_\mathrm{u} = p_\mathrm{b}(t) = \begin{cases} \sin^2(\pi t), & 0 \leqslant t \leqslant 1 \\ 0, & t > 1 \end{cases} \quad \text{at } z = 1 \tag{7}$$

together with the initial condition that $A(z, 0) = 1$. Equation (6b) states how the pressure within the renal pelvis (equal to p_u at $z = 0$) increases (decreases) with time as fluid flows into (out of) the renal pelvis. Equation (7) states that the pressure at $z = 1$ is equal to the bladder pressure.

From equation (4b) it can be seen that p_s depends on p_u. Substituting the expressions for p_u and p_s into equation (5a), it is straightforward to show that equation (4a) is a non-linear diffusion equation for A, with diffusion coefficient D. For large values of D, corresponding to long pressure pulse durations, the pressure and the ureter cross-sectional area are expected to be approximately independent of the axial coordinate z. For small values of D, the pressure pulse (7) that drives flow into the ureter from the bladder does not reach the renal pelvis before the bladder pressure starts to decrease again. The ureter wall then relaxes so that the amplitude of the fluid pulse decreases, with some fluid moving towards the kidney and some towards the bladder. Over sufficiently long times (compared with the duration of the bladder pressure pulse) the fluid returns to the bladder.

For a given prescribed bladder pressure pulse, the reflux volume at each end of the ureter is a function of time, defined to be

$$\int_0^t q(z, t')\,\mathrm{d}t' \tag{8}$$

where the values at the UPJ and VUJ are taken by setting $z = 0$ and $z = 1$ respectively. In the above, q is given by equation (5a). Note that negative values of q indicate reflux, and hence reflux figures will be quoted as negative numbers. The total reflux at the UPJ is the volume of fluid entering the renal pelvis from the ureter and the total reflux at the VUJ is the volume of fluid entering the ureter from the bladder.

These are determined by the minimum over time of equation (8) at $z = 0$ and $z = 1$ respectively.

The governing equations (4) are solved numerically subject to the boundary condition (6) and (7) and an initial condition. The spatial derivatives are approximated using standard second-order-accurate finite difference approximations and the resulting system of coupled ordinary differential equations is solved using the method of lines. The code is validated by refining the mesh, increasing the error tolerances, and also by comparing steady state solutions against asymptotic predictions (see reference [**9**] for full details).

2.3 Parameter values

To determine the typical size of the dimensionless parameters and provide insight into the system dynamics, representative parameter values must be given. The viscosity μ^* is 6.54×10^{-3} g/cm s and the density ρ^* is $1\,\mathrm{g/cm^3}$ [**10**]. The ureter length l^* is 25 cm [**8**] and the natural cross-sectional area $A_a^* = \pi(0.2)^2\,\mathrm{cm^2}$, so that the aspect ratio is $\sqrt{A_a^*/\pi}\big/l^* = 8\times10^{-3}$. The inner and outer stent cross-sectional areas are $A_i^* = \pi(6.5)^2\times10^{-4}\,\mathrm{cm^2}$ and $A_o^* = \pi(9.5)^2\times10^{-4}\,\mathrm{cm^2}$ respectively, measured from stents supplied by Boston Scientific. Additionally, the stent permeability, d^*, based on the number and size of holes in the stent wall, is estimated to be $1.6\times10^{-3}\,\mathrm{cm^3/g\,s}$ [**9**].

To the authors' knowledge, values for the parameters k^* and γ in the expression for the ureter membrane tension (1) and for the renal pelvis bulk stiffness, k_k^*, in the stented human are unavailable, although data do exist for porcine and canine (unstented) ureters [**12**, **13**]. In the absence of such data, k^* is considered to be set by the requirement that the reduced Reynolds number is small. The reduced Reynolds number is given by $\varepsilon^2\mathcal{U}^*l^*\rho^*/\mu^*$, where $\varepsilon = \sqrt{A_a^*/\pi}/l^*$ is the aspect ratio and $\mathcal{U}^*$ is a typical axial velocity scale, which is determined via a balance of viscous stress and axial pressure gradient in the axial momentum equation. The size of the fluid pressure, P^*, is determined by the typical wall stiffness and radius, and $P^* \sim k^*/\sqrt{A_a^*/\pi}$ (see equation (1)). It is then straightforward to show that $\mathcal{U}^* \sim k^*\sqrt{A_a^*/\pi}/(\mu^*l^*)$ and that the reduced Reynolds number is $k^*\rho^*(A_a^*)^{3/2}\big/\left(l^{*2}\mu^{*2}\pi^{3/2}\right)$; requiring this to be much smaller than one the present authors set $k^* = 1\times10^{-3}$cm (cm H_2O). The present authors also consider k and k_k to be $O(1)$, and set $k_k^* = 2\times10^{-3}(\mathrm{cm\ H_2O})\mathrm{cm^{-3}}$ and take values for $P_{b,max}^*$ in the range $1\text{–}5\times10^{-3}$ cm H_2O. Finally, to ensure that changes in area due to increased bladder pressure are $O(1)$ the authors consider $\gamma = 2.5$. Future experimental work is required to ascertain the sizes of these material parameters, particularly in the stented system where k^* is expected to be lower than for healthy ureters owing to the loss of muscle tone associated with stenting [**14**].

2.4 Results

The parameter values used in the following results are given in section 2.3. Typical flows are illustrated that were obtained for long pulse duration (D large) and short pulse duration (D small) respectively. Note that the non-dimensionalization is such that the dimensionless pulse duration and the dimensionless amplitude of the prescribed bladder pressure pulse are both 1.

A start is made by considering $P_{b,max}^* = 5\times10^{-3}$ cm H_2O and $\tau^* = 5\times10^3$ s. In this case, $D \approx 30$. In Fig. 3(a) the pressure within the stent, $p_s(z, t)$ is shown (note that p_u may be determined using equation (5b)), and in Fig. 3(b) the corresponding ureter cross-sectional area, $A(z, t)$, is illustrated. The prescribed bladder pressure (the pressure profile at $z = 1$) is denoted by the dashed black line in Fig. 3(a). Initially, the bladder and renal pelvis reduced pressures are both zero, the ureter is at its natural cross-sectional area of 1, and there is no flow. As the reduced bladder pressure increases from zero, the ureter rapidly inflates and p_k increases owing to reflux through the UPJ. The size of D is such that an axially uniform state is quickly achieved.

Next, shorter pulses are considered with $P_{b,max}^* = 5\times10^{-3}$ cm H_2O and $\tau^* = 100$ s. Figure 3(c) shows the pressure profile within the stent and Fig. 3(d) the corresponding ureter cross-sectional area A. For this case, $D \approx 1$, and an axially uniform profile is not observed for A or p_s. As the bladder pressure increases, a pulse of fluid flows into the ureter and the cross-sectional area increases close to the downstream end ($z = 1$). However, the duration of the prescribed bladder pulse is such that the fluid pulse does not have time to reach the UPJ ($z = 0$) before the bladder pressure starts to decrease. The ureter wall then relaxes, with some fluid flowing towards the renal pelvis and some towards the bladder. Again, over sufficiently long times all the fluid returns to the bladder.

These contrasting flow behaviours are reflected in the reflux volumes. In Fig. 4, the volume of fluid

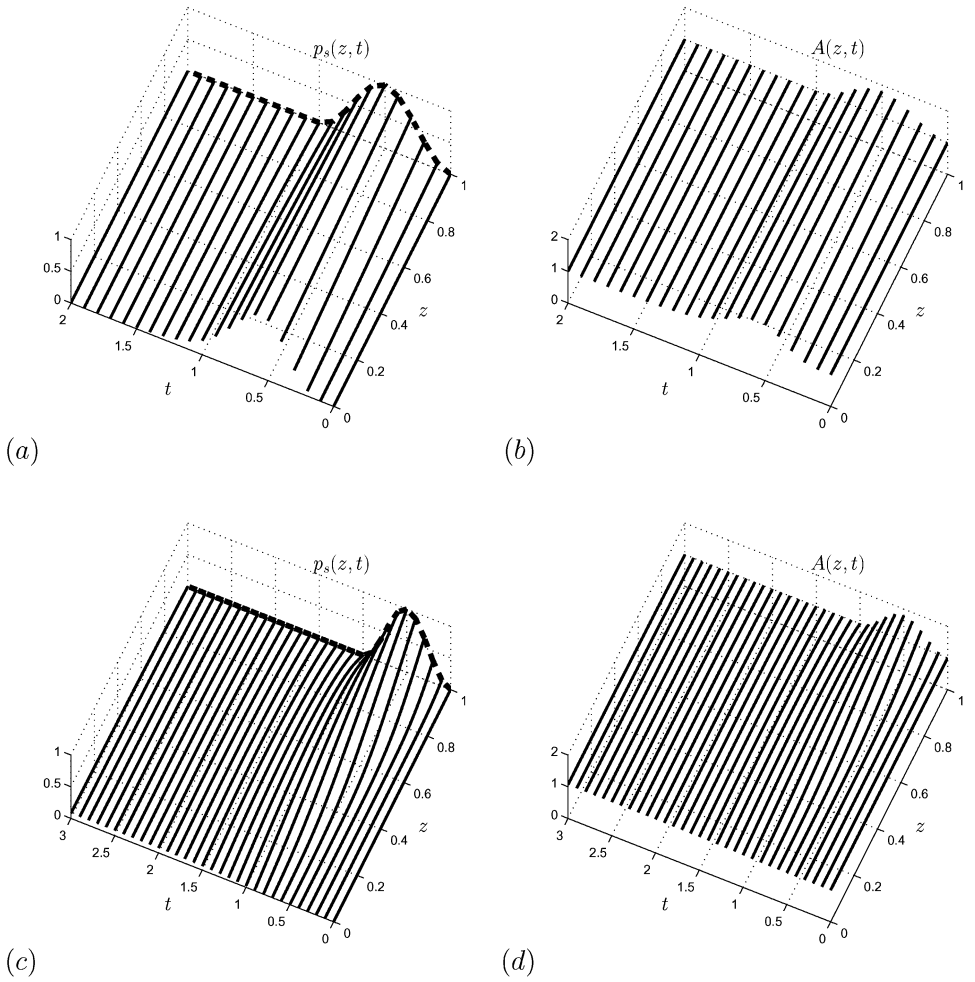

Fig. 3 In all figures $P^*_{b,max} = 0.005$ cm H_2O. In Figs (a) and (b), $\tau^* = 5\times10^3$ s and in Figs (c) and (d), $\tau^* = 100$ s. Figures (a) and (c) show the pressure within the stent $p_s(z, t)$ and Figs (b) and (d) show the ureter cross-sectional area $A(z, t)$

entering the ureter from the bladder (dashed line) and the volume leaving the ureter and entering the renal pelvis (solid line) are plotted as a function of t for the scenarios considered above. The black circle indicates the total reflux volume into the renal pelvis, and the black square, the total reflux volume from the bladder into the ureter. In each case, the reflux into the ureter from the bladder exceeds that from the ureter into the renal pelvis. For the longer duration pulse, the times at which the two reflux maxima are achieved are approximately equal and occur just after half-way through the pulse duration. This behaviour is due to the large diffusion coefficient, which causes time-dependent variations in bladder pressure to be rapidly transmitted to the renal pelvis. For the shorter duration pulse, there is a delay before significant reflux is observed in the renal pelvis; this is a consequence of the fact that for a smaller value of D a pulse of fluid travels up the ureter towards the renal pelvis on the timescale of the prescribed bladder pressure rise. The timescale over which the equilibrium state is restored (and the reflux volumes return to zero) is much longer than the duration of the prescribed pressure pulse.

In Fig. 5, the total reflux into the renal pelvis and into the ureter from the bladder as a function of the pulse duration, τ^*, are plotted for several values of $P^*_{b,max}$. The large black circles correspond to the total reflux values found in the simulations shown in Fig. 4 (corresponding to $P^*_{b,max} = 0.005$ cm H_2O and $\tau^* = 100$ s and 5×10^3 s). Note that the choices of $P^*_{b,max}$ and τ^* used in Fig. 4 illustrate the extremes of behaviour, though of course smaller pulse durations (more realistic physiologically) can be considered. Moreover, while the pressure rises considered here are small, the degree of total reflux is significant, highlighting that it is important to minimize the potential irritation of the bladder by stents (which can lead to transient rises in bladder pressure) when considering their design.

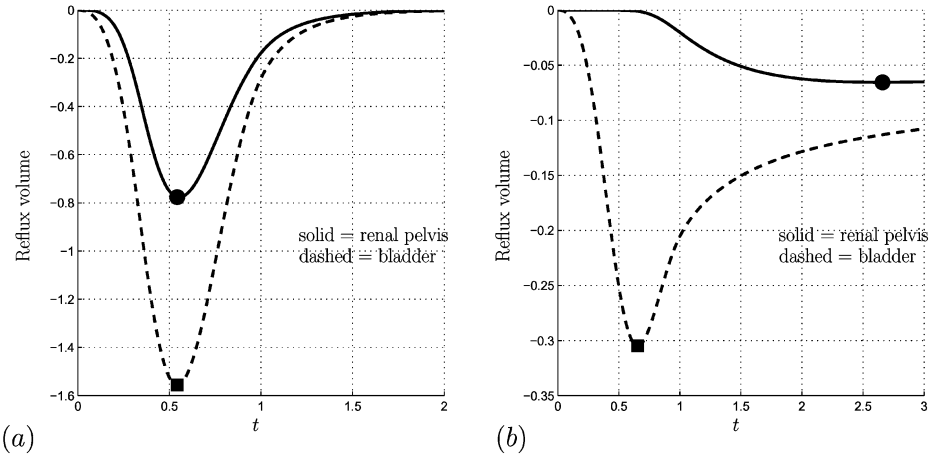

Fig. 4 Reflux volume as a function of time given by equation (8). (a) $P^*_{b,max} = 0.005$ cm H_2O and $\tau^* = 5 \times 10^3$ s, (b) $P^*_{b,max} = 0.005$ cm H_2O and $\tau^* = 100$ s. In each figure, the solid line denotes the reflux volume into the renal pelvis and the dashed line the reflux volume from the bladder into the ureter. The solid black circle denotes the maximum reflux volume (total reflux) into the renal pelvis and the solid black square the maximum reflux volume (total reflux) into the ureter from the bladder

For fixed τ^* it can be seen that increasing the amplitude of the pressure pulse results in an increase in the total reflux, as expected. For a fixed pressure amplitude, the total reflux is a monotonically increasing function of the pulse duration τ^*. For small τ^*, the pressure pulse entering the ureter from the bladder does not reach the renal pelvis before the bladder pressure starts to decrease again, and the reflux is small. For large values of τ^*, the total reflux at the renal pelvis asymptotes to the value $-1/k_k$. This may be explained as follows. Large values of τ^* correspond to large values of D. In this regime the pressure within the stent is approximately axially uniform and is given by the value of the bladder pressure $p_b(t)$. From equation (6b), the flux at the renal pelvis is then given by $-(\partial p_b/\partial t)/k_k$, and hence the total reflux (obtained by integrating over the duration for which p_b is increasing in time) is $-1/k_k$. A similar argument gives the total reflux at the bladder to be $(1-\mathcal{A})-1/k_k$, where $\mathcal{A}$ is the solution to $k\{\exp[\gamma(\sqrt{\mathcal{A}}-1)]-1\}/\sqrt{\mathcal{A}}=1$.

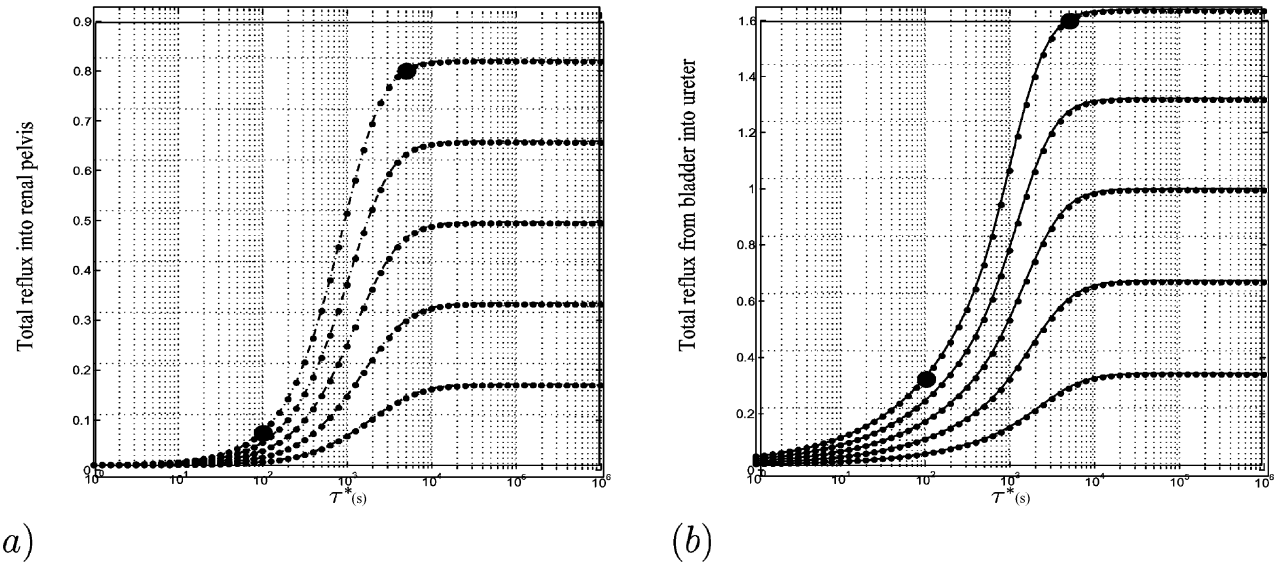

Fig. 5 Graph of the total reflux into (a) the renal pelvis and (b) the ureter, against pulse duration, τ^*. In both figures, $P^*_{b,max}$ increases from 0.001 to 0.005 cm H_2O. In each figure, the lowest curve represents the lowest value of $P^*_{b,max}$. The large filled black circles indicate the parameter values for the scenarios in Figs 3 and 4

3 URETERIC STENT ENCRUSTATION

It is generally assumed that the mechanism underlying ureteric stent and urethral catheter encrustation is the same. Urethral catheters, which drain urine from the bladder to the external environment, have a tendency to become blocked by encrustations [**15**, **16**]. These encrustations arise as a result of the presence of the bacterial species *Proteus mirabilis*, which releases an enzyme (urease) causing an increase in the urinary pH [**17**, **18**]. This in turn induces crystals of triple phosphate to precipitate on the catheter surface. These can grow to a size that blocks the catheter and restricts urine flow. The aim is to determine if the same mechanism explains ureteric stent encrustation.

3.1 Methodology

An extensive survey was undertaken of the bacterial flora associated with ureteric stents removed from patients treated in the urology unit of Nottingham City Hospital. The double-pigtail stents (Percuflex® Plus Ureteral Stent, Boston Scientific, Natick, Massachusetts) were collected immediately after removal from the patient. Of 52 stents examined, 29 were from female patients and 23 from males. The age of patients ranged from 21 to 82 years, with an average of 55 years. The period for which these had been in place varied considerably between patients, from 6 to 453 days. The stents were transported in purpose-built sterile Perspex boxes. They had a channel hollowed into the rectangular base in the shape of a stent which prevented cross-contamination of the surface by microbes from other areas; e.g. those bacteria attached to the surface of the lower (bladder) end of the stent were prevented from coming into contact with those that adhered to the surface of the upper (kidney) end. The stents were stored at 4 °C and analysed within 24 hours of their removal.

The stents were aseptically removed from the box and placed on a sterile surface, where they were examined and photographed. Three areas of the stent were sampled: the upper and lower ends and a section of the middle part. A 2–3 cm length was sampled depending on the degree of encrustation. Stents were assessed visually as either clean, discoloured (yellow, brown, or black), coated in a thin white powdery layer, or encrusted; see Fig. 6 for examples of typical encrustations.

The stent sections were immediately placed in 2.5 mL of 0.25 per cent Ringers solution (Oxoid, Basingstoke) and sonicated for 30 minutes to dislodge any attached bacteria/encrustation from the surfaces. The sonicate was used to make a slide preparation, which was heat fixed and stained by gram stain. This was examined for tissue, protein, and other debris, and for white blood cells (mono- or polynuclear), bacteria, and yeasts. The sonicate was used to perform semi-quantitative streak plates in triplicate on blood agar (Oxoid, Basingstoke) (for the culture of fastidious and other types of organism) and MacConkey agar (minus NaCl) (Oxoid, Basingstoke) (for the culture of coliforms while suppressing the swarming of *Proteus* spp.). After 24–36 hours incubation at 37 °C, the colonies were counted and noted according to their colonial appearance. Re-

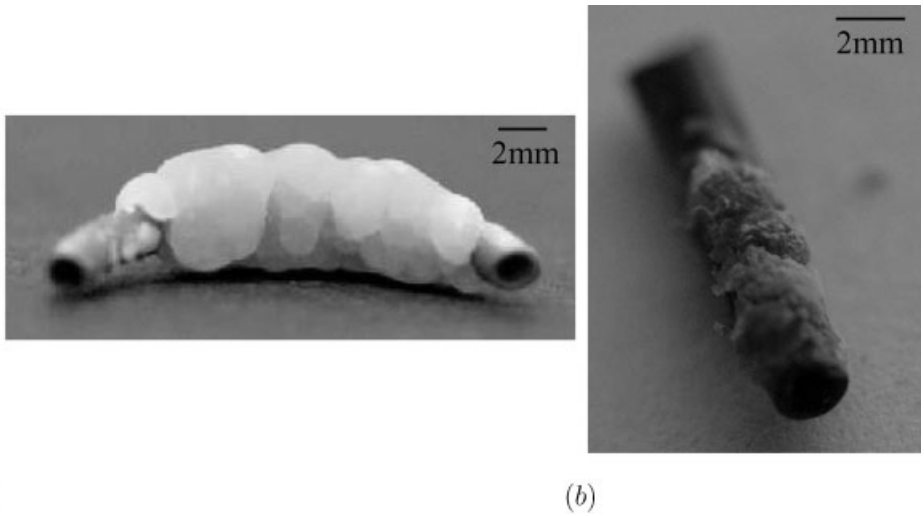

Fig. 6 Section of encrustation from the region of the stent residing in the bladder: (a) stent resident for 58 days (female, 21 years); (b) stent resident for 196 days (male, 44 years)

presentative colonies of each type were counted and then picked off the plates and subcultured on to the appropriate medium as streaks to ensure purity. Once pure cultures had been established, they were gram stained and a decision was made at this stage of their probable identity based on their colonial and gram appearances and the medium on which they grew. Supplementary tests such as oxidase, catalase, and DNAse tests were also undertaken. According to these results, the appropriate API test (bioMérieux, Basingstoke) was used to identify the bacterial species. All yeasts were identified using API Candida.

3.2 Results

Although 18 bacterial and 4 yeast species were isolated, *P. mirabilis* was not isolated from any of the stents. The ability of each bacterial species to produce urease was tested using three techniques: (a) as part of the biochemical tests within the API bacterial identification systems; (b) by growth on Christensen's urease agar (Oxoid, Basingstoke); and (c) by growth in a modified urea broth (phosphate buffered saline, 0.1 g/L yeast extract, 20 g/L urea, and 0.01 g/L phenol red) to induce urease production in those species capable of utilizing urea as a substrate. It was found that isolates from seven species of bacteria were capable of producing urease (*Comamonas acidovorans*, *Klebsiella pneumoniae*, *Pseudomonas aeruginosa*, *Staphylococcus aureus*, *S. epidermidis*, *S. warneri*, *S. xylosus*, *Escherichia coli*, *Morganella morganii*, and *Enterobacter* spp.). However, it took a considerable length of time before the *Escherichia, Klebsiella*, and *Pseudomonas* isolates began to produce urease in order to gain carbon for growth, which suggests that they preferentially utilize another source. *M. morganii* is the only rapid producer of urease but it was only isolated twice from brown discoloured stents. All types of encrustation were found in the presence and absence of all species of bacteria, and bacteria were isolated from encrustation-free stents. Therefore, the data revealed no direct correlation between the presence of any of the bacterial species and any type of encrustation. In summary, encrustations were found in the absence of bacterial species, in the presence of non-urease producing species, and in the presence of urease-producing species.

4 DISCUSSION

The present authors have highlighted features of their interdisciplinary work to understand the causes of ureteric stent failure. The paper concludes with a summary of the work and brief details are given by the ongoing work in this area.

4.1 Urine flow in stented ureter

A theoretical model for reflux in a stented ureter when the bladder pressure increases was developed. It was found that both increasing the duration and amplitude of the bladder pulse resulted in a significant increase in reflux up to a fixed threshold value (see the end of section 2.4) that can be predicted. This simplified model does not account for urine production by the kidney, changing elasticity of the ureter wall, or axial variations in the stent wall thickness due to encrustation. These features are examined in a more detailed model presented in reference [**9**]. The model provides an insight into the flow dynamics within a stented ureter, and moreover will be used to inform experimental design, e.g. when recreating the *in vivo* flow conditions *in vitro*, in experiments to understand how the local flow environment can influence subsequent stent encrustation.

4.2 Ureteric stent encrustation

The present study focused on the possibility of a link between the presence of bacteria and encrustation, and is the first to elaborate the bacterial flora present on ureteric stents *in vivo*. It has been established that, in contrast to urethral catheters, ureteric stent encrustation does not depend on the presence of the urease-producing *P. mirabilis*, and indeed, can occur in the absence of any bacteria. One current focus of activity of stent manufacturers is the development of antimicrobial stents, e.g. by impregnating the stent biomaterial with targetted antibiotics. This study demonstrates that this approach may not prevent encrustation and that focusing on *P. mirabilis* is probably misguided.

In patients with urethral catheters, attempts have been made to use dietary means to control the patient's urinary environment, i.e. to neutralize the alkinalizing effect of the urease on the urine pH, to minimize encrustation *in vivo* (see reference [**17**] and references therein). However, these have generally failed owing to the ability of *P. mirabilis* to produce a high concentration of urease rapidly. Given that the authors have established that only weak urease-producing bacterial species are found in association with ureteric stents, it is hypothesized that ureteric stent encrustation could be prevented

through controlling the urinary environment. To be able to do this, there is first a need to establish the environment in which the encrustations on the removed stents developed. Since all the stents are of the same material, and therefore have a similar pH nucleation point, then any differences in the crystal structure and chemical composition of the encrustations could be correlated with the local urine environment. Therefore, a detailed examination of the crystal structure and chemical composition within the encrustation may prove useful.

To achieve this, a combination of techniques is used, such as electron probe microanalysis (EPMA), X-ray diffraction (XRD), energy dispersive X-ray analysis (EDX), scanning electron microscopy (SEM), and X-ray photoelectron spectroscopy (XPS). These can be used to elucidate the physical appearance, chemical elements, bonding type, and structure of the crystals. The crystals and amorphous structures on the surface have a variety of geometries and chemical composition. Correlation of such structures for both thick encrustations, as depicted in Fig. 6, and thin deposits, as observed on other stents, with patient data and chemical and physical information, forms the basis of ongoing work. Additionally, this work will be complemented by experimentally validated theoretical predictions from a model of the encrustation process on the surface of a stent. The model will account for the critical conditions under which crystal nucleation occurs and the subsequent crystal growth [**19**].

Future experimental work will recreate the *in vivo* flow regime experienced by a ureteric stent, informed by theoretical studies of the flow dynamics in a stented ureter [**9**]. A novel experimental rig has been developed which has enabled encrustation development on actual stents to be assessed. The local environment is manipulated and subsequent encrustation development is determined on representative biomaterials, enabling predictions to be made as to how the local environment must be controlled *in vivo* to prevent ureteric stent encrustation.

CONCLUSIONS

This multidisciplinary project has quantified the degree of reflux that can arise in a stented ureter, identified the microbial species found in association with ureteric stents after their removal from patients, and characterized these strains to ascertain whether they have the ability to alter the local environment to a state that induces the nucleation of crystals in the urine and ultimately the growth of encrustation on the stent surface. Ongoing work is examining the detailed crystal structure and chemical composition of the encrustations, which will inform future work in which encrustation in carefully controlled environments is studied [**20**, **21**]. Interdisciplinary work of this nature is leading to exciting developments in the understanding of the causes of ureteric stent failure, and the insight gained is invaluable in the future design of stents that minimize the degree of reflux and encrustation.

ACKNOWLEDGEMENTS

The authors gratefully acknowledge support from the BBSRC (JHS and KH) and an EPSRC Advanced Research Fellowship (SLW).

REFERENCES

1 **Nancollis, G. H.** Crystallisation theory relating to urinary stone formation. *World J. Urol.*, 1983, **1**, 131–137.
2 **Cahill, D. J., Fry, C. H.,** and **Foxall, P. J. D.** Variation in urine composition in the human urinary tract: evidence of urothelial function *in situ*. *J. Urol.*, 2003, **3**, 871–874.
3 **Shafik, A., Ahmed, I., Sibai, O. E.,** and **Shafik, A. A.** Does the composition of voided urine reflect that of the renal pelvis? *Urol. Res.*, 2006, **34**, 261–264.
4 **Seymour, H.** and **Patel, U.** Ureteric stenting – current status. *Sem. Intervent. Radiol.*, 2000, **17**, 351–366.
5 **Finney, R. P.** Experience with new double-j ureteral catheter stent. *J. Urol.*, 1978, **120**, 678–681.
6 **Dyer, R. B., Chen, M. Y., Zagoria, R. J., Regan, J. D., Hood, C. G.,** and **Kavanagh, P. V.** Complications of ureteral stent placement. *RadioGraphics*, 2002, **22**, 1005–1022.
7 **Pate, U.** and **Kellett, M. J.** Ureteric drainage and peristalsis after stenting studied using colour doppler ultrasound. *Br. J. Urol.*, 1996, **77**, 530–535.
8 **Cummings, L. J., Waters, S. L., Wattis, J. A. D.,** and **Graham, S. J.** The effect of ureteric stents on urine flow: reflux. *J. Math. Biol.*, 2004, **19**, 56–82.
9 **Siggers, J. H., Cummings, L. J., Waters, S. L.,** and **Wattis, J. A. D.** Flow dynamics in a stented ureter. *Math. Med. Biol.*, 2008 (submitted for publication).
10 **Batchelor, G. K.** *An introduction to fluid dynamics*, 1967 (Cambridge University Press, Cambridge).
11 **Fung, Y. C.** Elasticity of soft tissues in simple elongation. *Am. J. Physiol.*, 1967, **213**, 1532–1544.
12 **Hebert, L. A., Stuart, K. A.,** and **Stemper, J. A.** Whole kidney volume/pressure relationships. *Kidney Int.*, 1975, **7**, 45–54.

13 **Gregerson, H., Knudsen, L., Eika, B., Frøkiær, J.,** and **Djurhuus, J. C.** Regional differences exist in elastic wall properties in the ureter. *Scand. J. Urol. Nephrol.*, 1996, **30**, 343–348.
14 **Ramsey, J. W. A., Payne, S. R., Gosling, P. T., Whitfield, H. N., Wickham, J. E. A.,** and **Levison, D. A.** The effects of double-j stenting on unobstructured ureters – an experimental and clinical study. *Br. J. Urol.*, 1985, **57**, 630–634.
15 **Reid, G., Tieszer, C., Denstedt, J.,** and **Kingston, D.** Examination of bacterial and encrustation deposition on ureteral stents of differing surface properties, after indwelling in humans. *Colloid. Surf. B: Bioint.*, 1995, **5**, 171–179.
16 **Faqih, R. S., Shamsuddin, A. B.,** and **Chakrabarti, A.** Polyurethane ureteral stent in treatment of stone patients: morbidity related to indwelling times. *J. Urol.*, 1991, **146**, 1487–1491.
17 **Morris, N. S.** and **Stickler, D. J.** The effect of urease inhibitors on the encrustation of urethral catheters. *Urol. Res.*, 1998, **26**, 275–279.
18 **Stickler, D. J., Ganderton, L., King, J.,** and **Winters, C.** *Proteus mirabilis* biofilms and the encrustation of urethral catheters. *Urol. Res.*, 1993, **21**, 407–411.
19 **Siggers, J. H., Wattis, J. A. D., Cummings, L. J.,** and **Waters, S. L.** Mathematical model of catheter encrustation, 2008 (in preparation).
20 **Band, L. R., Cummings, L. J., Waters, S. L.,** and **Wattis, J. A.** Crystal aggregation and deposition in the catheterised lower urinary tract. *J. Math. Biol.*, 2008 (submitted for publication).
21 **Heaton, K., Neate, N., Bayston, R., Bishop, M.,** and **Grant, D. M.** Characterisation of types of explant ureteric stent encrustation, 2008 (in preparation).